

Space Weather



RESEARCH ARTICLE

10.1029/2020SW002692

Key Points:

- Cross-calibration analysis between Arase/XEP and RBSP/MagEIS & REPT measurements and validation using two different ESA radiation monitors
- Harmonization of science-class energetic electron flux measurements define reference data set(s) for the outer Van Allen belt
- Reference data sets to be used for the harmonization of radiation monitors and the update/validation of climatological and space weather models

Correspondence to:

I. Sandberg,
sandberg@sparc.gr















Citation:

Sandberg, I., Jiggins, P., Evans, H., Papadimitriou, C., Aminimalragia-Giamini, S., Katsavrias, C., et al. (2021). Harmonization of RBSP and Arase energetic electron measurements utilizing ESA radiation monitor data. *Space Weather*, 19, e2020SW002692. <https://doi.org/10.1029/2020SW002692>

Received 6 DEC 2020

Accepted 6 APR 2021

Harmonization of RBSP and Arase Energetic Electron Measurements Utilizing ESA Radiation Monitor Data

Ingmar Sandberg¹ , Piers Jiggins² , Hugh Evans² , Constantinos Papadimitriou¹ , Sigiava Aminimalragia-Giamini¹ , Christos Katsavrias^{1,3} , Alexander J. Boyd⁴ , Thomas Paul O'Brien⁴ , Nana Higashio⁵ , Takefumi Mitani⁵ , Iku Shinohara⁵ , Yoshizumi Miyoshi⁶ , Daniel N. Baker⁷ , and Ioannis A. Daglis^{3,8} 

¹Space Applications & Research Consultancy, Athens, Greece, ²European Space Agency, European Research and Technology Centre, Noordwijk, The Netherlands, ³Department of Physics, National and Kapodistrian University of Athens, Athens, Greece, ⁴Aerospace Corporation, Chantilly, VA, USA, ⁵Japan Aerospace Exploration Agency, Tsukuba, Japan, ⁶Institute for Space-Earth Environmental Research, Nagoya University, Nagoya, Japan, ⁷Laboratory for Atmospheric and Space Physics, Boulder, CO, USA, ⁸Hellenic Space Center, Athens, Greece

Abstract Accurate measurements of trapped energetic electron fluxes are of major importance for the studies of the complex nature of radiation belts and the characterization of space radiation environment. The harmonization of measurements between different instruments increases the accuracy of scientific studies and the reliability of data-driven models that treat the specification of space radiation environment. An intercalibration analysis of the energetic electron flux measurements of the Magnetic Electron Ion Spectrometer (MagEIS) and the Relativistic Electron-Proton Telescope (REPT) instruments on-board the Van Allen Probes (VAP) Mission versus the measurements of the Extremely High Energy Electron Experiment (XEP) unit on-board Arase satellite is presented. The performed analysis demonstrates a remarkable agreement between the majority of MagEIS and XEP measurements and suggests the rescaling of MagEIS HIGH unit and of REPT measurements for the treatment of flux spectra discontinuities. The proposed adjustments were validated successfully using measurements from ESA Environmental Monitoring Unit (EMU) on-board GSAT0207 and the Standard Radiation Monitor (SREM) on-board INTEGRAL. The derived results lead to the harmonization of science-class experiments on-board VAP (2012–2019) and Arase (2017–) and propose the use of the data sets as reference in a series of space weather and space radiation environment developments.

Plain Language Summary Accurate measurements of trapped energetic electron fluxes are of major importance for the studies of the complex nature of radiation belts and the characterization of space radiation environment. The harmonization of measurements between different instruments increases the accuracy of scientific studies and the reliability of data-driven models that treat the specification of space radiation environment. This study leads to the harmonization of the relativistic electron flux data sets from the cornerstone US and Japanese Radiation Belt missions. The derived results are validated by European Space Agency radiation monitors and can be used in a series of applications and developments.

1. Introduction

The dynamics of the Earth's magnetosphere provide an efficient mechanism for the trapping and the acceleration of energetic particles. At the Earth's magnetic equator, the outer belt extends from an altitude of just over 10,000 km to distances beyond geostationary orbit and is dominated by trapped electrons. The electron peak flux is energy-dependent but is typically at an orbit altitude between 3.5 and 5 Earth radii at the magnetic equatorial plane. The relativistic electron population in the outer Van Allen radiation belt is extremely variable—especially during periods of enhanced geomagnetic activity—as it is subjected to processes, such as loss and acceleration, which compete and can deplete or enhance electron populations (Reeves et al., 2016; Turner et al., 2015). For satellites, the outer belt poses a significant hazard since the intense electron fluxes cause ionizing dose, nonionizing energy loss, and internal charging. For a better understanding of the physical mechanisms associated with the dynamics of the outer belt it is critical to have accurate flux measurements of the trapped energetic electrons. This case is usually met in the high-energy resolution

© 2021. The Authors.

This is an open access article under the terms of the [Creative Commons Attribution License](https://creativecommons.org/licenses/by/4.0/), which permits use, distribution and reproduction in any medium, provided the original work is properly cited.

measurements of detectors that constitute part of scientific experiments. Such data sets are usually considered as reference for the in-flight evaluation and calibration of radiation monitors on-board other satellites. The use of cross-calibrated measurements—under a common reference—can be vital for the derivation of coherent model outputs from data-driven engineering models that treat the characterization of the space radiation environment (O'Brien et al., 2018). One such example is the Solar Energetic Particle Environment Modelling reference data set (SEP-EM RDS) (Heynderickx et al., 2018), based on NOAA GOES proton flux measurements (Onsager et al., 1996), cross-calibrated by Sandberg et al. (2014) using as reference the IMP-8 Goddard Medium Energy experiment (Richardson et al., 2008). SEP-EM RDS has resulted to the production of spectrally coherent outputs in various solar energetic proton environment models (Aminalragia-Giamini et al., 2018; Jiggins et al., 2018). For the case of the trapped radiation environment, cornerstone missions that carry science-class electron detectors—after the CRRES era (1990–1991) (Johnson & Kierein, 1992)—are the Radiation Belts Storm Probes (RBSP) (Mauk et al., 2012) and more recently the Exploration of energization and Radiation in Geospace (ERG) (Miyoshi, Shinohara, et al., 2018).

We distinguish here the science-class particle detectors from the particle radiation monitors. The former ones are developed with the primary goal to serve the scientific needs of the mission they participate in by providing measurements with specially tailored characteristics—such as uni-directional, high energy, and temporal resolution—that can reveal characteristics of the physical mechanisms linked to the goals of the mission. The latter ones are designed to provide reliable, long-term, and robust measurements for the monitoring of the radiation environment with the main goal of the protection and the evaluation of any radiation effects encountered at the satellite subsystems but with omni-directional measurements with lower energy and temporal resolution.

The RBSP are twin spin-stabilized spacecraft assigned with the study of the radiation belts and the inner magnetosphere. The probes were launched in August 2012 in near-equatorial highly elliptic orbit (HEO) with 10.2° inclination and a period of ~9 h (perigee at 618 km and apogee about 30,000). RBSP-B was deactivated in July 2019 and RBSP-A 3 months later. The electron data analysis from the science class detectors Magnetic Electron Ion Spectrometer (MagEIS) (J. B. Blake et al., 2013) and Relativistic Electron-Proton Telescope (REPT) (D. N. Baker et al., 2012) on-board RBSP led to a series of investigations and breakthrough discoveries (D. N. Baker et al., 2014; Mann et al., 2016), related to the electron belt dynamics and the physical mechanisms responsible for electron losses and energization. The ERG mission is a newer science mission, developed by JAXA in collaboration with universities and institutes in Japan and Taiwan, aiming to study electron acceleration and loss mechanisms in the outer radiation belt. The mission was launched in December 2016 and initiated its scientific observations 3 months later in elliptic orbit with 31° inclination and a period of ~8 h (perigee at 400 km and apogee at 32,000 km). Arase carries, among others, the extremely high-energy electron experiment (XEP) (Higashio et al., 2018a), which provides electron flux measurements at energies above 0.3 MeV.

In this study, we have performed and validated successfully an intercalibration of the electron flux measurements of MagEIS and REPT versus those of XEP—utilizing measurements from two ESA radiation monitors. The resulting harmonized data sets can be considered as reference for use in a series of application and models; for the calibration of space radiation detectors on-board satellites, the orbits of which cross the HEO of RBSP and Arase, for the building/evaluation of quantitative climatological/engineering models, and for the development/validation of radiation belt forecasting space weather models. Section 2 presents the characteristics of the data sets considered and Section 3 presents the derivation of the harmonization factors accounting for RBSP data sets. In Section 4, a validation study is presented using the deep charging current measurements of the Environmental Monitoring Unit (EMU) (Sandberg et al., 2019) on-board Galileo satellite GSAT207 and the measurements from Standard Radiation Monitor (SREM) (Mohammadzadeh et al., 2003) on-board INTEGRAL (Evans et al., 2008).

2. RBSP and Arase Electron Flux Measurements

MagEIS and REPT instruments are part of the Energetic Particle Composition and Thermal Suite (ECT) (Spence et al., 2013). MagEIS utilizes a strong magnet to steer electrons into a set of solid-state detectors (SSDs), providing flux measurements of ~30 keV to 4 MeV (Blake et al., 2013). MagEIS consists of four units:

Table 1
Scaling Factors for the Harmonization of ECT to XEP Electron Fluxes; Quiet Magnetospheric Conditions Were Considered for the Channels With $E < 3$ MeV

MagEIS energy channels			
E [MeV]	Median	$s f \min(MSE)$	Conjunctions
0.176	1.03	1.04	140
0.217	–	–	0
0.240	0.97	0.88	406
0.350	0.98	0.90	405
0.470	0.99	0.94	370
0.600	0.94	0.93	307
0.749	0.94	0.91	294
0.904	0.87	0.86	190
1.064	1.35	1.30	215
1.072	–	–	0
1.575	1.37	1.38	262
1.728	1.23	1.22	259
2.254	1.23	1.27	87
2.589	1.51	1.72	62
3.536	0.84	0.73	73
3.970	1.79	1.71	58
REPT energy channels			
E [MeV]	Median	$s f \min(MSE)$	Conjunctions
1.9	4.52	3.87	422
2.1	2.22	2.20	369
2.6	1.80	2.00	251
3.4	2.21	1.97	652
4.2	1.91	1.65	400
5.2	2.37	2.31	322
6.3	1.45	1.43	91
7.7	0.29	0.24	12
9.9	1.07	1.07	1

the LOW measures low-energy electrons (~ 30 – 200 keV), two MEDIUM units measure electrons of ~ 200 keV to 1 MeV, and the HIGH measures relativistic electrons (~ 1 – 4 MeV). We have used the background-corrected Level-2 Release-4 spin-averaged flux MagEIS data sets (Claudepierre et al., 2015). The energy values assigned to MagEIS channels in this study correspond to the mean values of the twin units (Table 1) accounting from August 3, 2013. For the derivation of the cross-calibration factors, we use measurements with background correction error (FESA_ERROR) above 50% similar to Boyd et al. (2019).

REPT uses a stack of SSD and provides relativistic electrons measurements in 10 channels, the energy efficiency of which is characterized by long “tails” (D. N. Baker et al., 2012). The derivation of the REPT electron differential fluxes—within 1.9–12.3 MeV—was performed using the bow-tie analysis method (Van Allen et al., 1974). The present study demonstrates results for the channels up to 9.3 MeV (Table 1). We have analyzed the Level-2 Release-3 data sets which include background measurements induced by the galactic cosmic rays. For the subset of measurements that overlap Arase ones, the background level was estimated for each channel—using a cutoff threshold as it did not present significant modulations—and subtracted. For the needs of the harmonization studies, a 3-min time-averaged ECT data set was created to match the resolution of XEP measurements.

XEP unit (Higashio et al., 2018a) includes a detection system that contains five SSDs that measure electrons in the energy range of 0.4–5.4 MeV. The first SSD is 50 μm thick, while the others are 1,500- μm thick. An aluminum shield (130- μm thick) is placed in front of the first SSD to prevent the intrusion of light and electrons with $E < 0.4$ MeV. The present study is based on the use of Level-2 version 01-00 electron omni-directional fluxes binned in nine energy channels—within a time period from March 20, 2017 to August 31, 2019. The measurements of each channel were assigned to the geometric mean of its energy bin boundaries $E_{XEP} = (0.55, 0.69, 0.89, 1.09, 1.34, 1.64, 1.98, 2.48, \text{ and } 3.13)$ MeV.

3. Harmonization of ECT and XEP Data Sets

The comparisons between ECT and XEP electron measurements are based on the determination of suitable conjunctions between the orbits of the carrier satellites. The conjunctions may be defined as the spatio-temporal positions where the detectors are expected to encounter the same population of trapped electrons. For the determination of these positions, we followed the spirit of the recommendations of the Panel on Radiation Belt Environment Modeling (Bourdarie et al., 2008) but required stricter criteria for the spatiotemporal conditions, namely $\delta L \leq 0.01$, $\delta(\alpha_{eq}) \leq 2^\circ$, $\delta t \leq 1$ h. Here, L denotes the L-shell value and α_{eq} the equatorial pitch angle. On the contrary, we completely relaxed the conditions related to the magnetic local time MLT —by setting $\delta(MLT) \leq 12$ h—to have the largest possible number of conjunctions for the aforementioned strict criteria. The magnetic coordinates were derived using the UNILIB library (Heynderickx et al., 2000) assuming the IGRF model for the internal, and the quiet Olson-Pfizer 1977 (Olson & Pfizer, 1977) model for the external magnetic field components.

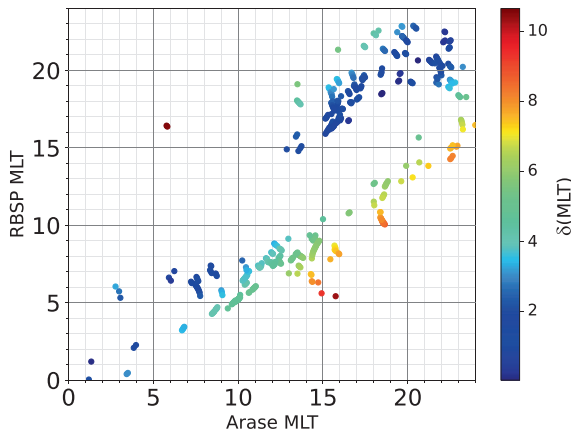


Figure 1. Cross-plot of the Magnetic Local Times of Arase and RBSP missions during the “quiet” conjunctions which were adopted for the harmonization of ECT energetic channels with $E < 3$ MeV.

The application of these criteria resulted to 2,853 magnetic conjunctions within $4.3 \leq L \leq 6.5$. However, by imposing the additional criterion for quiet magnetospheric conditions, that is, $K_p < 2$ for the last 2 days (Bourdarie et al., 2008)—defined from now on as the “quiet” conjunctions—the number of conjunctions was reduced to 510. As it will be shown later on, the “quiet” conjunctions were selected for the calibration of the $E < 3.0$ MeV ECT channels. In Figure 1, we present the Magnetic Local Times of the considered missions for the “quiet” conjunctions; the 95% had $\delta(MLT) < 7.8$, the 75% had $\delta(MLT) < 5.0$ and the 50% had $\delta(MLT) < 3.5$ h.

For the flux comparisons, we rebinned XEP fluxes to the ECT energies. For the values within the XEP energy range, a piece-wise power-law interpolation was applied and for extrapolating the values below (or above), a performed non-linear least square fitting was performed using the first (or last) three points of each XEP flux spectrum. As a fit function, we used an exponential cutoff power-law. The errors associated with the use of the piece-wise power-law interpolation may be considered insignificant given the dense energy binning of XEP. However, the uncertainties resulted from the extrapolation increase as we move further from XEP

energy range even though the selected fit function is able to capture both exponential and power-law behavior as well as all the in-between cases. As it will be discussed later on, this can become evident for the conjunctions considered during disturbed times—where the selected fit function may not be adequate to describe the electron flux spectra at energies below 0.55 MeV. In addition, errors could possibly arise when extrapolating background measurements of XEP ultra-relativistic energy channels. However, these cases were identified and excluded from the following analysis.

This procedure allowed us to perform quantitative comparisons between the rebinned XEP f_{XEP} and the ECT energetic fluxes f_{ECT} . In Figure 2, we present box-and-whisker plots of the flux ratios (f_{ECT} / f_{XEP}) created using the Seaborn plot Python library (Waskom & the seaborn development team, 2020). The boxes show the quartiles of the flux ratios, the upper and the lower horizontal lines indicate the upper and the lower quartiles while the median is displayed by the horizontal line inside. The whiskers extend to show the rest of the distribution. The yellow boxes correspond to the available spatiotemporal conjunctions and the blue ones to the “quiet” conjunctions. The box-and-whiskers for the MagEIS comparisons (upper plot) indicate a remarkable agreement between the calibration of XEP and MEDIUM channels ($E < 1$ MeV) which becomes evident when the quiet magnetospheric conditions are considered (i.e., blue boxes). For $1.06 \leq E \leq 2.59$ MeV, MagEIS/HIGH and XEP channels differ by a factor of less than two, while the differences between yellow and blue box-and-whiskers are not significant.

On the other hand, the differences between the two box-and-whiskers become important at $E \leq 0.47$ MeV. Here, we must note that this feature is prominent to channels that are not included in the XEP energy range and are thus extrapolated. Nevertheless, and even though the aforementioned extrapolation may contribute to the differences between quiet and disturbed times, we believe that these differences are rather physics-based and depend on the MLT asymmetry that is pronounced at the seed (a few hundreds of keV) electron fluxes. This MLT dependence becomes more prominent during disturbed periods of the geospace as the seed electrons are directly modulated by the substorm activity and/or the enhanced magnetospheric convection.

The differences which appear for the last two HIGH channels, for $E > 3.5$ MeV, are attributed to the drastic decrease of the available ultra-relativistic electron flux measurements during quiet conjunctions. The box-and-whisker plot accounting for the REPT comparisons (lower plot) reveals a consistent difference with XEP—of the order of two—for the energies at $2.1 \leq E \leq 6.3$ MeV, while the deviation at 1.9 MeV is larger. For $E \leq 6.3$ MeV, the differences between blue and yellow box-and-whiskers are not significant. For the channels above 6.5 MeV, however, measurements of ultra-relativistic electrons appear only during active magnetospheric conditions.

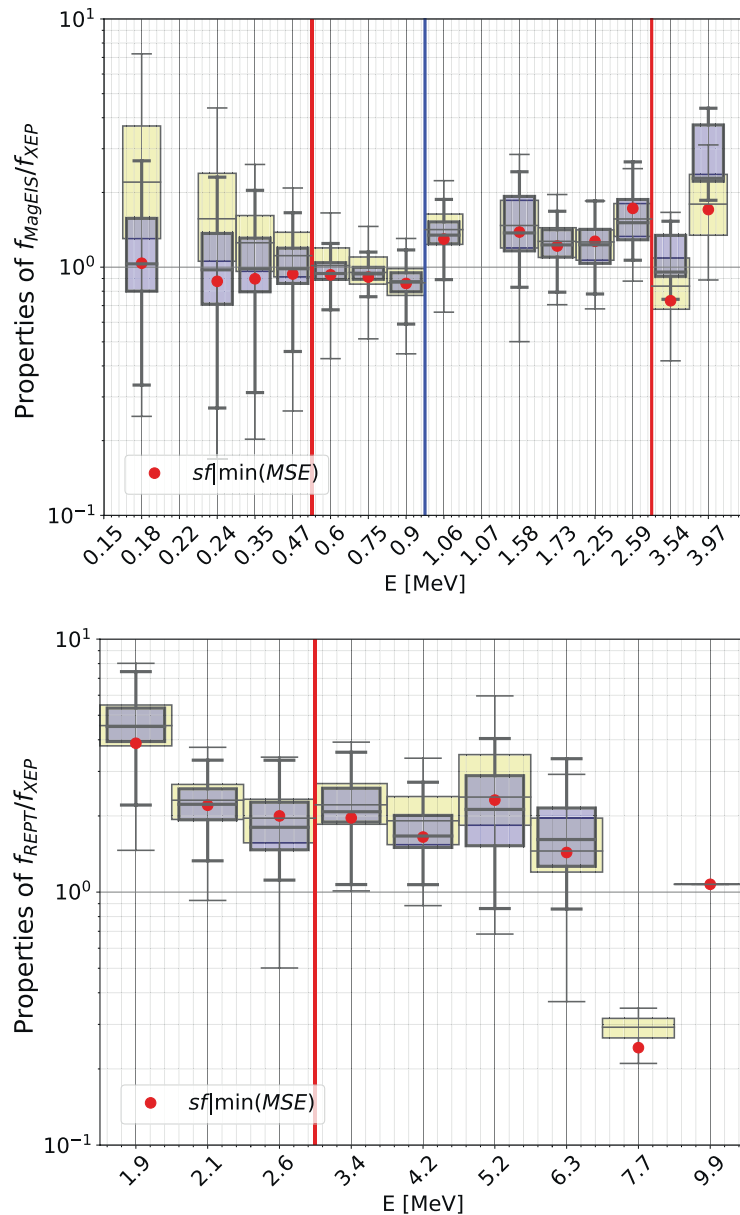


Figure 2. Box-and-whiskers for the ratios $f_{\text{MagEIS}}/f_{\text{XEP}}$ (upper plot) and $f_{\text{REPT}}/f_{\text{XEP}}$ (lower plot). The yellow boxes include the measurements during the spatiotemporal conjunctions and the blue boxes—with the thick whiskers—to “quiet” conjunctions. The blue line perpendicular to the energy axis separates the MEDIUM and the HIGH channels. The red line(s) define the ECT channels that fall within the XEP energy range. The red circles denote the values that—when divide the ECT fluxes—achieve an MSE minimization with the rebinned XEP fluxes when all (quiet) conjunctions are considered for $E > 3$ ($E < 3$) MeV. The box-and-whiskers for the MagEIS energy channels 0.22 and 1.07 MeV are missing due to the absence of measurements. ECT, MSE, mean squared error.

In view of the above, we conclude that the use of the “quiet” conjunctions is appropriate only for the derivation of the scaling factors for the ECT channels below 3.0 MeV. The scaling factors, may be defined either as the median values of the ratios ($f_{\text{ECT}} / f_{\text{XEP}}$), or as the factors that minimize the mean squared error (MSE) between f_{XEP} and f_{ECT} series, defined here as $sf \mid \min(\text{MSE})$. Table 1 lists these values, together with the number of the available conjunction measurements used for each energy channel.

Figure 3 presents—as example—cross-plots between the rescaled ECT f_{ECT}/sf and the rebinned f_{XEP} fluxes for the 0.47 MeV MagEIS and the 6.3 MeV REPT channels. Note that the 0.47 MeV is the nearest MagEIS en-

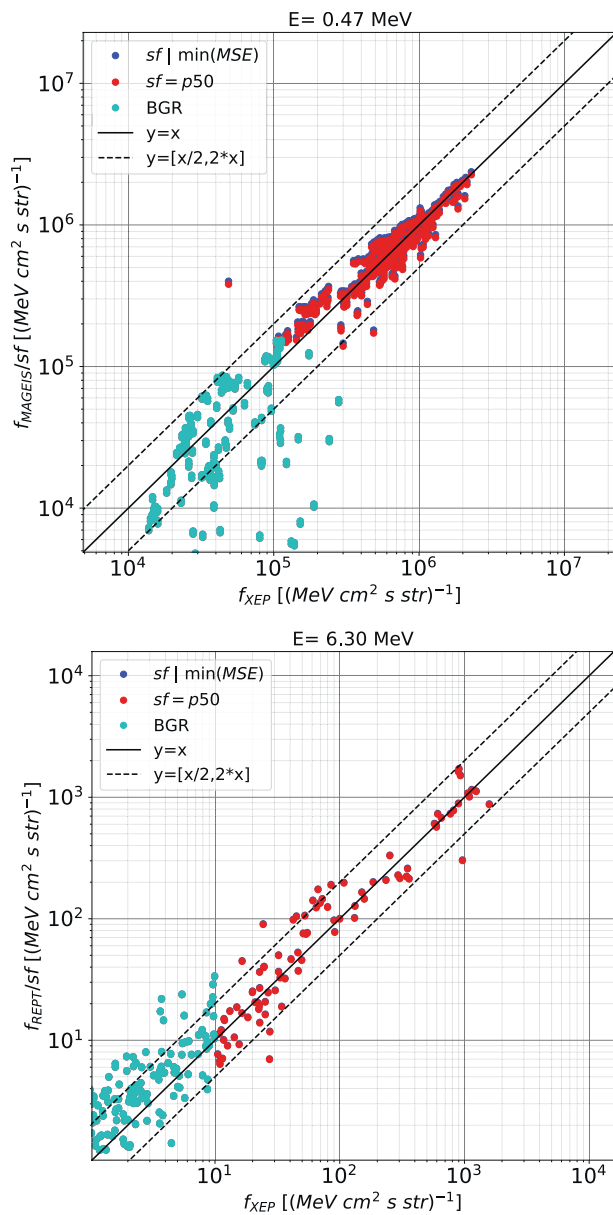


Figure 3. Cross plots between the re-scaled MagEIS (REPT) electron differential fluxes versus the interpolated XEP fluxes rebinned at 0.47 MeV (6.30 MeV) using the quiet (all the) spatio-temporal conjunctions. The red circles correspond to the ECT fluxes divided by the median value (P50) and the blue by the factor $sf|_{min(MSE)}$. The cyan circles denote flagged measurements, that is, with large statistical error or within the background, which were not considered in the derivation of the scaling factors.

ergy channel just outside the XEP energy range and the 6.3 MeV channel is the highest in energy channel that was possible to cross-calibrate. The ECT adjustments have been performed by dividing either by the *median* or by the $sf|_{min(MSE)}$ values (cf. Table 1). Note that measurements with large statistical error or within the background (cf. Section 2)—which were not taken into account in the calculation of the adjustment factors—are also included in these plots.

The derived results demonstrate a remarkable agreement between MEDIUM and XEP measurements and suggest the rescaling of MagEIS/HIGH and REPT measurements. The proposed adjustments, as listed in Table 1, lead to the harmonization of the science-class high energy experiments on-board RBSP (2012–2019) with Arase (2017–). The differences between the rescaling factors for MagEIS/MEDIUM, MagEIS/HIGH, and REPT units can be attributed to the different calibration procedures applied separately for each unit and to the increased background of the last HIGH channel. The performed studies also indicate the necessity for relaxing the K_p -related restrictions (Bourdarie et al., 2008) for the cross-calibration of relativistic electron flux measurements; during quiet magnetospheric conditions, the measured fluxes are typical of low intensity and below the instrument’s background levels. Last, but not least, it should be noted that REPT team has recently found a missing factor of two in the data processing software. Next data releases will address this issue (communication with Shri Kanekal, NASA) resulting in an improved agreement with XEP.

4. Validation of Data Harmonization

4.1. ESA Radiation Monitors

For the validation of the ECT adjustments suggested by XEP comparisons, we utilized measurements from ESA radiation monitors on-board missions, the orbits of which cross the near-equatorial HEO of RBSP. Such conditions are met by the EMU on-board Galileo satellites and the ESA SREM on-board INTEGRAL mission. Both of these sensors have been calibrated by means of GEANT4 simulations (Agostinelli et al., 2003) and provide healthy measurements. The EMU is a radiation sensitive instrument designed for use in the orbit of the GNSS Galileo constellation. Two units are currently flying; the first one is on-board GSAT0207, launched in November 2016, while the second unit is on board GSAT0215, launched in December 2017. EMU includes a SURF sensor (Ryden et al., 2015), composed of a stack of eight charge collecting plates that measure internal charging currents. The unit is mounted on the spacecraft panel with a view in the East-West direction, for example, $\sim 90^\circ$ pitch angle. SURF data have been used for the creation of differential electron flux data set within 0.2–8.0 MeV by Sandberg et al. (2019). Here, we use the primary internal charging current measurements from the last four GSAT0207/EMU/SURF plates utilizing the response function derived by modeling the shielding impact of the host spacecraft by

a Ta slab of 5-cm thickness. SREM unit consists of three SSD in a two-detectors-head configuration and measures electrons with $E > 0.5$ MeV and protons with $E > 10$ MeV. SREM samples have electron fluxes in rather broad and overlapping energy bands providing measurements in 15 channels. The units on-board STRV-1C, Rosetta, GIOVE-B, Herschel, and Planck spacecraft have completed their operation while those on-board Proba-1 and INTEGRAL continue to provide healthy measurements after two decades. Here, we use the count-rate measurements from the INTEGRAL/SREM S12, S13, and C4 channels utilizing their

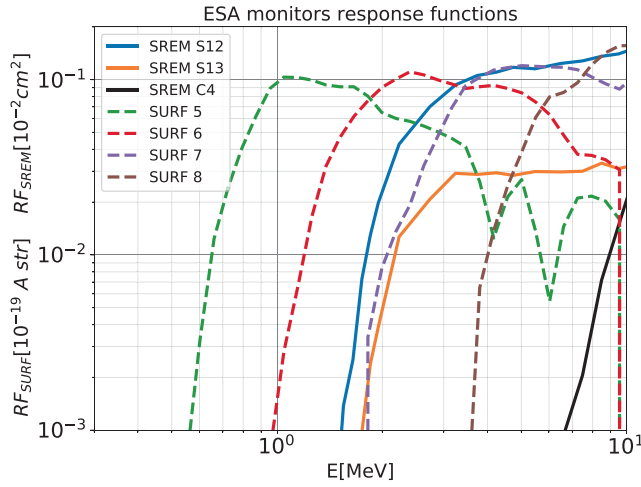


Figure 4. Electron response functions of INTEGRAL/SREM and GSAT0207/EMU selected channels.

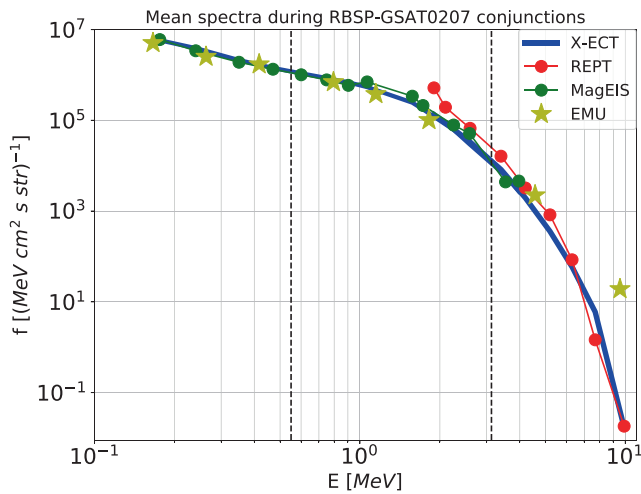


Figure 5. RBSP/ECT mean flux spectra during the conjunctions with GSAT0207. The rescaled spectrum (blue line) is presented versus the original MagEIS (green circles) and REPT (red circles) spectra. The mean flux spectrum of GSAT0207/EMU is also presented (gold stars).

Table 2
Summary of Validation Results Using ESA Radiation Monitor Data

Channel	$E_{25,50,75}$ [MeV]	$M'(C_{rec}/C)$	$M(C'_{rec}/C)$
SURF_5	1.4, 2.2, 3.4	1.4	1.2
SURF_6	2.6, 3.8, 5.0	2.3	1.3
SURF_7	3.9, 4.8, 5.7	1.9	1.1
SURF_8	5.2, 5.7, 6.2	1.8	1.0
SREM_S12	2.0, 2.3, 2.9	3.7	1.2
SREM_S13	2.1, 2.5, 3.0	3.4	1.2
SREM_C4	3.3, 3.7, 4.8	0.7	0.4

electron response functions for the derivation of which a mass model that included the host spacecraft was used. SREM is typically directed along a pitch angle of $\sim 90^\circ$. Figure 4 presents the electron response functions of the channels selected from both ESA radiation monitors.

4.2. Validation Approach and Results

The validation approach considered is to compare ECT and ESA radiation monitor measurements before and after the application of the XEP-induced scaling factors $sf_{min}(MSE)$. The spatiotemporal conjunctions were determined using the same criteria presented in Section 3; 1,830 RBSP conjunctions were found with GSAT0205 and 830 with INTEGRAL.

Figure 5 presents the mean electron flux spectra of ECT and EMU for the RBSP-GSAT207 conjunctions. It is evident that the rescaling of ECT data treats the mismatches between MagEIS/MEDIUM, MagEIS/LOW, and REPT calibrations leading to coherent spectra over four orders of magnitude. We note that these adjustments may be particularly important in phase space density calculations which are sensitive on the flux spectrum slope. It is worth-mentioning that the adjusted ECT spectrum seems to exhibit two breaks at ~ 0.3 and ~ 1.8 MeV which is consistent with the three-step scenario (Jaynes et al., 2015; Katsavrias et al., 2019) to describe the different acceleration mechanisms from seed (100–300 keV), to relativistic (up to 2 MeV) and ultra-relativistic (>2 MeV) electrons. The bow-tie derived EMU spectra are found to be in very good agreement, up to 5 MeV, according to Sandberg et al. (2019). It remains still the question if the proposed adjustments lead to improvements in terms of the absolute flux values per se. To confirm that, we fold the ECT fluxes $f(E)$ with the response function RF_i of each monitors' channel i ;

$$C_{rec,i} = \int_0^{E_{max}} f(E)RF_i(E)dE, \quad (1)$$

and calculate the reconstructed measurements $C_{rec,i}$. The latter ones were compared with the actual measurements C_i using the median values of their ratios $M(i) = median(C_{rec,i}/C_i)$. For the case of SURF plates, MagEIS and REPT spectra were merged to construct $f(E)$, while for SREM, only the REPT spectra were considered. The same procedure was repeated for the calculation of the median values $M'(i)$ derived using the rescaled ECT fluxes. The modification in the median values accounting for the reconstructed measurements is presented in Table 2; the median values for SURF plates 5–8, reached values closer to one after the rescaling. The same trend was also observed for the case of SREM channels as well.

In support to the above, we calculated for each channel the value of the upper energy integration limit E_{max} in Equation 1 that contributes to the 25%, 50%, and 75% of the reconstructed data—for the indicative case of the mean flux spectra. The corresponding values $E_{25,50,75}$ [MeV] are included in Table 2 and allow us to determine the “effective” electron energy range responsible for the differences between $M(i)$ and $M'(i)$ with respect to the rescaled ECT fluxes. Note that the “effective” electron energy range depends on the synergy of the response function and the differential electron flux spectra. We found that the agreement accounting for the

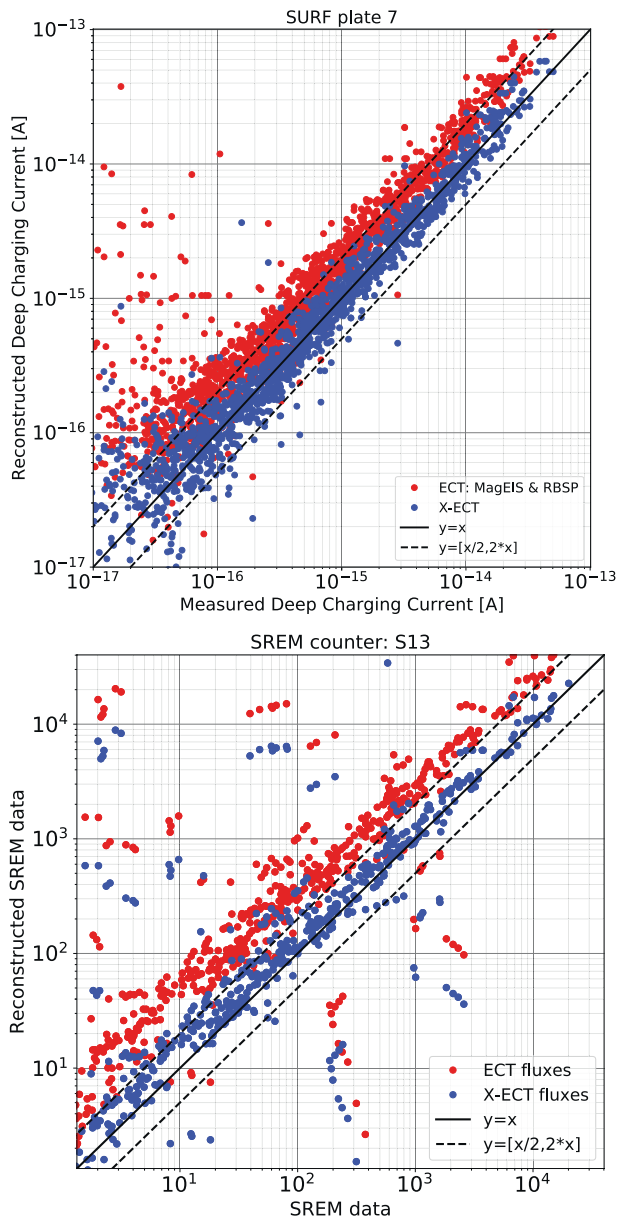


Figure 6. Actual measurements of SURF plate 7 (upper plot) and SREM channel S13 (lower plot) versus reconstructed ones as derived by folding the electron response function with the ECT spectra before (red dots) and after (blue dots) the harmonization of the ECT spectra.

SURF plates 5–8 was attributed to the re-scaling(s) within the 2–6 MeV range while the improvement accounting for SREM_S12 and S13 channels was attributed to the adjustments within the 2–3 MeV. Given these consistent agreements, the change in the median values accounting for SREM_C4 channel—which found to be attributed to adjustments within 3.3–4.8 MeV—can be only justified by the statistically poor resolution of channel’s response at this energy range (cf. Figure 4). Figure 6 present—as characteristic examples—the cross-plots between $C_{rec,i}$ and $C'_{rec,i}$ for the case of SURF_7 and SREM_S13 channels.

These results validate the harmonization between ECT and XEP relativistic and ultra-relativistic electron flux measurements at least for the energies up to 6.3 MeV. In addition, they demonstrate the calibration consistency between ESA radiation monitors and XEP. Note, however, that the impact of the presented cross-calibration work is essentially quantified in Table 1 and secondarily in the adjustments of M to M' values in Table 2 which validate in a type of cumulative sense the results of Table 1, that is, through the folding of the differential fluxes with the radiation monitor response functions (cf. Equation 1).

5. Applications

The harmonization of science-class experiments on-board RBSP and Arase defines an extended reference baseline for the relativistic electron flux measurements from 2012. A reference data set with the characteristics presented in the previous sections can be used in a series of applications. Space radiation monitors on-board satellites, the orbits of which have crossed the HEO of RBSP and Arase can be cross-calibrated under a reference. A typical example to be considered is the case of the MEO radiation measurements from the monitoring units on-board GNSS constellations such as the EU Galileo and the US GPS. In addition, even monitors at GEO can be cross-calibrated as long as they were operating during the Geostationary Transfer Orbit of the carrier satellite. The use of the harmonized relativistic data sets can also contribute to the development or evaluation of quantitative climatological/engineering models based on a large number of different data sets. In such models, like the IRENE (O'Brien et al., 2018), it is important to adopt a reference baseline and use it to identify and eliminate the systematic biases in the considered data sets, and also to quantify their observational uncertainties. Last, a reference megaelectron-volt electron flux data set with measurements that span almost a decade can be used for the improvement or the validation of physical or data-driven (Bourdarie & Maget, 2012; Glauert et al., 2014; Subbotin & Shprits, 2009), predictive electron radiation belt models leading to improved forecasts accounting the state of the outer belt.

6. Conclusions

Systematic disagreements in the calibration of trapped energetic electron flux measurements can be crucial for scientific studies based on synergistic observations of energetic electrons and for the outputs of space radiation environment specification models. In this study, we proceeded to the intercalibration of Arase/XEP and RBSP/ECT measurements. For the harmonization of ultra-relativistic electron fluxes, the criterion of using quiet magnetospheric conditions for the determination of conjunctions was relaxed. The remarkable agreement between XEP and the majority of MagEIS channels was demonstrated, together with the suggestion of adjusting MagEIS/HIGH and REPT measurements accordingly. The harmonization factors

for the ECT channels were derived and validated—for at least up to ~ 6 MeV—using measurements from ESA radiation monitors. For $E > 6$ MeV, extended investigations will be carried out using GSAT/EMU measurements. The harmonization of cornerstone electron flux measurements defines an extended reference baseline that can be used in a series of applications; for the calibration of space radiation detectors, for updating/validating quantitative climatological and/or forecasting models addressing the electron radiation environment of the outer Van Allen belt.

Data Availability Statement

The authors acknowledge Bern Blake, Joe Fennell, Seth Claudepierre, and Drew Turner for the use of MagEIS data and Dan Baker, Shri Kanekal, Alyson Jaynes for the use of the REPT data. RBSP-ECT data are publicly available at <http://www.RBSP-ect.lanl.gov/>. Science data of the Arase (ERG) satellite were obtained from the ERG Science Center operated by ISAS/JAXA and ISEE/Nagoya University (Miyoshi, Hori, et al., 2018). The present study used the Level-2 (version 01-00) data from the XEP experiment on-board the Arase (ERG) satellite (Higashio et al., 2018b). The XEP data processing was partly supported by the SEES/JAXA. GSAT/EMU data are available to users from European member states registered at <https://gssc.esa.int/>. INTEGRAL/SREM data are publicly available at <http://srem.psi.ch/>.

Acknowledgments

The study has received funding from the European Union's Horizon 2020 research and innovation program "SafeSpace" under Grant agreement number 870437 and from the European Space Agency under the "European Contribution to International Radiation Environment Near Earth (IRENE) Modelling System" activity under ESA Contract number 4000127282/19/NL/IB/gg.

References

- Agostinelli, S., Allison, J., Amako, K., Apostolakis, J., Araujo, H., Arce, P., et al. (2003). Geant4—A simulation toolkit. *Nuclear Instruments and Methods in Physics Research Section A: Accelerators, Spectrometers, Detectors and Associated Equipment*, 506(3), 250–303. [https://doi.org/10.1016/s0168-9002\(03\)01368-8](https://doi.org/10.1016/s0168-9002(03)01368-8)
- Aminalragia-Giamini, S., Sandberg, I., Papadimitriou, C., Daglis, I. A., & Jiggins, P. (2018). The virtual enhancements – Solar proton event radiation (VESPER) model. *Journal of Space Weather and Space Climate*, 8, A06. <https://doi.org/10.1051/swsc/2017040>
- Baker, D. N., Jaynes, A. N., Hoxie, V. C., Thorne, R. M., Foster, J. C., Li, X., et al. (2014). An impenetrable barrier to ultrarelativistic electrons in the van allen radiation belts. *Nature*, 515(7528), 531–534. <https://doi.org/10.1038/nature13956>
- Baker, D. N., Kanekal, S. G., Hoxie, V. C., Batiste, S., Bolton, M., Li, X., et al. (2012). The Relativistic Electron-Proton Telescope (REPT) Instrument on Board the Radiation Belt Storm Probes (RBSP) Spacecraft: Characterization of Earth's radiation belt high-energy particle populations. *Space Science Reviews*, 179(1–4), 337–381. <https://doi.org/10.1007/s11214-012-9950-9>
- Blake, J. B., Carranza, P. A., Claudepierre, S. G., Clemmons, J. H., Crain, W. R., Dotan, Y., et al. (2013). The Magnetic Electron Ion Spectrometer (MagEIS) Instruments Aboard the Radiation Belt Storm Probes (RBSP) Spacecraft. *Space Science Reviews*, 179(1–4), 383–421. <https://doi.org/10.1007/s11214-013-9991-8>
- Bourdarie, S. A., & Maget, V. F. (2012). Electron radiation belt data assimilation with an ensemble Kalman filter relying on the Salammbó code. *Annales Geophysicae*, 30(6), 929–943. <https://doi.org/10.5194/angeo-30-929-2012>
- Bourdarie, S., Blake, B., Cao, J., Friedel, R., Miyoshi, Y., Panasyuk, M., & Underwood, C. (2008). *Data analysis procedure v1.2*. COSPAR. Retrieved from http://craterre.onecert.fr/prbem/Data_analysis.pdf
- Boyd, A. J., Reeves, G. D., Spence, H. E., Funsten, H. O., Larsen, B. A., Skoug, R. M., et al. (2019). RBSP-ECT combined spin-averaged electron flux data product. *Journal of Geophysical Research: Space Physics*, 124(11), 9124–9136. <https://doi.org/10.1029/2019ja026733>
- Claudepierre, S. G., O'Brien, T. P., Blake, J. B., Fennell, J. F., Roeder, J. L., Clemmons, J. H., et al. (2015). A background correction algorithm for Van Allen Probes MagEIS electron flux measurements. *Journal of Geophysical Research: Space Physics*, 120(7), 5703–5727. <https://doi.org/10.1002/2015ja021171>
- Evans, H. D. R., Bühler, P., Hajdas, W., Daly, E. J., Nieminen, P., & Mohammadzadeh, A. (2008). Results from the ESA SREM monitors and comparison with existing radiation belt models. *Advances in Space Research*, 42(9), 1527–1537. <https://doi.org/10.1016/j.asr.2008.03.022>
- Glauert, S. A., Horne, R. B., & Meredith, N. P. (2014). Three-dimensional electron radiation belt simulations using the BAS Radiation Belt Model with new diffusion models for chorus, plasmaspheric hiss, and lightning-generated whistlers. *Journal of Geophysical Research: Space Physics*, 119(1), 268–289. <https://doi.org/10.1002/2013ja019281>
- Heynderickx, D., Kruglanski, M., Quaghebeur, B., Speelman, E., & Daly, E. J. (2000). An overview and discussion of SPENVIS, ESA's Space Environment Information System, and UNILIB, a Fortran library of magnetic field utilities. In *SAE technical paper series*. SAE International. Retrieved from <https://doi.org/10.4271/2000-01-2415>
- Heynderickx, D., Sandberg, I., & Jiggins, P. (2018). Solar energetic particle environment modelling reference dataset v2.1. *ESA Technical Note*. Retrieved from http://sepem.eu/help/SEPEM_RDS_v2-01.zip
- Higashio, N., Takashima, T., Shinohara, I., & Matsumoto, H. (2018a). The extremely high-energy electron experiment (XEP) onboard the Arase (ERG) satellite. *Earth Planets and Space*, 70(1). <https://doi.org/10.1186/s40623-018-0901-x>
- Higashio, N., Takashima, T., Shinohara, I., & Matsumoto, H. (2018b). *The XEP instrument level-2 omniflux data of exploration of energization and radiation in geospace (ERG) arase satellite*. Retrieved from <https://doi.org/10.34515/DATA.ERG-00001>
- Jaynes, A. N., Baker, D. N., Singer, H. J., Rodriguez, J. V., Loto'aniu, T. M., Ali, A. F., et al. (2015). Source and seed populations for relativistic electrons: Their roles in radiation belt changes. *Journal of Geophysical Research: Space Physics*, 120(9), 7240–7254. <https://doi.org/10.1002/2015ja021234>
- Jiggins, P., Heynderickx, D., Sandberg, I., Truscott, P., Raukunen, O., & Vainio, R. (2018). Updated model of the solar energetic proton environment in space. *Journal of Space Weather and Space Climate*, 8, A31. <https://doi.org/10.1051/swsc/2018010>
- Johnson, M. H., & Kierein, J. (1992). Combined release and radiation effects satellite (CRRES): Spacecraft and mission. *Journal of Spacecraft and Rockets*, 29(4), 556–563. <https://doi.org/10.2514/3.55641>

- Katsavrias, C., Sandberg, I., Li, W., Podladchikova, O., Daglis, I. A., Papadimitriou, C., et al. (2019). Highly relativistic electron flux enhancement during the weak geomagnetic storm of April–May 2017. *Journal of Geophysical Research: Space Physics*, *124*(6), 4402–4413. <https://doi.org/10.1029/2019ja026743>
- Mann, I. R., Ozeke, L. G., Murphy, K. R., Claudepierre, S. G., Turner, D. L., Baker, D. N., et al. (2016). Explaining the dynamics of the ultra-relativistic third Van Allen radiation belt. *Nature Physics*, *12*(10), 978–983. <https://doi.org/10.1038/nphys3799>
- Mauk, B. H., Fox, N. J., Kanekal, S. G., Kessel, R. L., Sibeck, D. G., & Ukhorskiy, A. (2012). Science objectives and rationale for the Radiation Belt Storm Probes mission. In *The Van Allen probes mission* (pp. 3–27). Springer US. https://doi.org/10.1007/978-1-4899-7433-4_2
- Miyoshi, Y., Hori, T., Shoji, M., Teramoto, M., Chang, T. F., Segawa, T., et al. (2018). The ERG science center. *Earth Planets and Space*, *70*(1). <https://doi.org/10.1186/s40623-018-0867-8>
- Miyoshi, Y., Shinohara, I., Takashima, T., Asamura, K., Higashio, N., Mitani, T., et al. (2018). Geospace exploration project ERG. *Earth Planets and Space*, *70*(1). <https://doi.org/10.1186/s40623-018-0862-0>
- Mohammadzadeh, A., Evans, H., Nieminen, P., Daly, E., Vuilleumier, P., Buhler, P., et al. (2003). The ESA Standard Radiation Environment Monitor program first results from PROBA-1 and integral. *IEEE Transactions on Nuclear Science*, *50*(6), 2272–2277. <https://doi.org/10.1109/TNS.2003.821796>
- O'Brien, T. P., Johnston, W. R., Huston, S. L., Roth, C. J., Guild, T. B., Su, Y., & Quinn, R. A. (2018). Changes in AE9/AP9-IRENE version 1.5. *IEEE Transactions on Nuclear Science*, *65*(1), 462–466. <https://doi.org/10.1109/TNS.2017.2771324>
- Olson, W. P., & Pfizter, K. A. (1977). Magnetospheric magnetic field modeling, annual scientific report. AFOSR Contract No. F44620-75-C-0033. Retrieved from. <https://doi.org/10.1109/tns.2019.2915686>
- Onsager, T., Grubb, R., Kunches, J., Matheson, L., Speich, D., Zwickl, R. W., & Sauer, H. (1996). Operational uses of the GOES energetic particle detectors. In E. R. Washwell, (Ed.), *GOES-8 and beyond*. SPIE. <https://doi.org/10.1117/12.254075>
- Reeves, G. D., Friedel, R. H. W., Larsen, B. A., Skoug, R. M., Funsten, H. O., Claudepierre, S. G., et al. (2016). Energy-dependent dynamics of keV to MeV electrons in the inner zone, outer zone, and slot regions. *Journal of Geophysical Research: Space Physics*, *121*(1), 397–412. <https://doi.org/10.1002/2015ja021569>
- Richardson, I., Cane, H., von Rosenvinge, T., & McGuire, R. (2008). IMP 8 GME energetic particle observations over three solar cycles. *International Cosmic Ray Conference*, *1*, 323–326.
- Ryden, K. A., Hands, A. D. P., Underwood, C. I., & Rodgers, D. J. (2015). Internal charging measurements in medium earth orbit using the SURF sensor: 2005–2014. *IEEE Transactions on Plasma Science*, *43*(9), 3014–3020. <https://doi.org/10.1109/TPS.2015.2416436>
- Sandberg, I., Aminalragia-Giamini, S., Provatas, G., Hands, A., Ryden, K., Heynderickx, D., et al. (2019). Data exploitation of new Galileo environmental monitoring units. *IEEE Transactions on Nuclear Science*, *66*(7), 1761–1769. <https://doi.org/10.1109/tns.2019.2915686>
- Sandberg, I., Jiggins, P., Heynderickx, D., & Daglis, I. A. (2014). Cross calibration of NOAA GOES solar proton detectors using corrected NASA IMP-8/GME data. *Geophysical Research Letters*, *41*(13), 4435–4441. <https://doi.org/10.1002/2014gl060469>
- Spence, H. E., Reeves, G. D., Baker, D. N., Blake, J. B., Bolton, M., Bourdarie, S., et al. (2013). Science goals and overview of the radiation belt storm probes (RBSP) energetic particle, composition, and thermal plasma (ECT) suite on NASA's Van Allen Probes Mission. *Space Science Reviews*, *179*(1–4), 311–336. <https://doi.org/10.1007/s11214-013-0007-5>
- Subbotin, D. A., & Shprits, Y. Y. (2009). Three-dimensional modeling of the radiation belts using the versatile electron radiation belt (VERB) code. *Space Weather*, *7*(10). <https://doi.org/10.1029/2008sw000452>
- Turner, D. L., O'Brien, T. P., Fennell, J. F., Claudepierre, S. G., Blake, J. B., Kilpua, E. K. J., & Hietala, H. (2015). The effects of geomagnetic storms on electrons in Earth's radiation belts. *Geophysical Research Letters*, *42*(21), 9176–9184. <https://doi.org/10.1002/2015gl064747>
- Van Allen, J. A., Baker, D. N., Randall, B. A., & Sentman, D. D. (1974). The magnetosphere of Jupiter as observed with Pioneer 10: 1. Instrument and principal findings. *Journal of Geophysical Research*, *79*(25), 3559–3577. <https://doi.org/10.1029/ja079i025p03559>
- Waskom, M., & the seaborn development team. (2020). *mwaskom/seaborn*. Zenodo. <https://doi.org/10.5281/zenodo.592845>